

RECOILED AND SPUTTERED RADIOACTIVE IMPURITIES IN 11 MEV PROTON-BASED F-18 PRODUCTION

Imam Kambali^{1*}, Hari Suryanto¹, Parwanto¹, Kardinah², Nur Huda², Ferdy D. Listiawadi²,
Herta Astarina², Ratu R. Ismuha²

¹Center for Radioisotope and Radiopharmaceutical Technology, National Nuclear Energy Agency
(BATAN), Puspiptek Area, Serpong, South Tangerang, Indonesia
²Dharmais Cancer Hospital, Jakarta, Indonesia

(Received: March 2017 / Revised: April 2018 / Accepted: February 2019)

ABSTRACT

One of the quality control measures in F-18 radionuclide production target concerns the impurities which might be present in the proton-irradiated enriched H₂¹⁸O target. In this investigation, proton irradiations of enriched water targets were theoretically simulated by the Stopping and Range of Ions in Matter (SRIM) 2013 codes, followed by experimental measurements. First, the SRIM-calculated data were employed to understand the origins of the recoiled and sputtered species. Using a portable Gamma Ray Spectroscopy System, recoiled and sputtered radioactive impurities were measured in the enriched water target following F-18 production using 11 MeV proton beams. The experimental results indicate that Havar window-originated Co-56 radionuclide and silver body-originated Ag-110m radioisotope were identified in the post-irradiated enriched H₂¹⁸O target. In addition, after passing the ¹⁸F solution through a column containing Quaternary Methyl Acetate (QMA) resin, none of the radionuclidic impurities were any longer observed to any great extent in the sample.

Keywords: Cyclotron; F-18 radionuclide; Gamma ray spectroscopy; Radionuclidic impurity; SRIM

1. INTRODUCTION

Over the past few years, Positron Emission Tomography (PET) has been one of the most applied modalities in nuclear medicine. It requires positron-emitting radionuclides, such as fluorine-18 (F-18) in the form of ¹⁸F-Fluorodeoxyglucose (¹⁸FDG), ¹⁸F-Fluoro-L-dopa (¹⁸FDOPA), and ¹⁸F-Fluoro-L-tyrosine ¹⁸F-FTYR (Xie, 2011; Je et al., 2012; Libert et al., 2014; Lemaire et al., 2015; Jung et al., 2016). Fluorine-18 can be produced via ¹⁸O(p,n)¹⁸F nuclear reaction, in which an enriched water (H₂¹⁸O) target is bombarded by relatively low to medium energy protons (Hjelstuen et al., 2011) in a target system. The target system usually consists of a target body made of silver and a Havar window separating the cyclotron chamber from the target (Kambali et al., 2010; Kambali et al., 2016), although a niobium (Nb)-based window has also been used (Köhler et al., 2013).

During proton beam irradiation, the beam has to pass through a Havar window before reaching the enriched water target; therefore, the Havar foil, which consists of cobalt (42.5%), chromium (20%), iron (18.1%), nickel (13%), tungsten (2.8%), molybdenum (2%), manganese (1.6%), carbon (0.2%), beryllium (0.04%) and some other trace elements, could become radioactive

*Corresponding author's email: imamkey@batan.go.id, Tel. +62-21-7563141, Fax. +62-21-7563141
Permalink/DOI: <https://doi.org/10.14716/ijtech.v10i2.3060>

atoms, depending on the proton energy. This occurrence could impact on quality control assessment, and from a broader perspective it could eventually give rise to patient safety concerns.

A previous investigation discovered that during routine production of F-18 radionuclide using 11 MeV proton beams, Co-56 radionuclide was generated via $^{56}\text{Fe}(p,n)^{56}\text{Co}$ nuclear reaction as the proton beam passed through the Havar window (Kambali et al., 2016). For higher proton energy (16.5 MeV), Bowden et al. (2009) observed other radionuclides such as V-48, Cr-51, Mn-52, Mn-54, Co-57, Co-58, Tc-95m, Tc-96, Cd-109, Re-183 and Re-184 in the Havar foil. Using Nb foil as the window separating the cyclotron vacuum chamber and enriched water target, Köhler et al. (2013) identified further radionuclides, including Zr-89, Nb-92m, Mo-93m, Tc-95 and Tc-96, when they irradiated the enriched water with 18 MeV protons.

Radionuclides generated during proton bombardment of Havar or Nb windows have previously been found to contaminate the enriched water target (Bowden et al., 2009; Hjelstuen et al., 2011; Köhler et al., 2013;). This work aims to comprehensively identify the recoiled and sputtered radionuclidic impurities during F-18 production using a relatively low (11 MeV) proton accelerating cyclotron. For the first time, the properties of the Havar window- and silver body-originated recoils are discussed in terms of their respective absorbed and kinetic energy after they experience collisions with the incoming proton beams, as well as their collisions with individual H and O atoms in the enriched water. In addition, the recoiled and sputtered yields are also highlighted based on the Stopping and Range of Ions in Matter (SRIM) calculated results.

2. EXPERIMENTAL METHODS

2.1. Irradiation

The target of interest for F-18 production was 97% purity enriched water (H_2^{18}O), purchased from Cambridge Isotope Laboratories Ltd. Nearly 1.8 ml of the enriched water target was placed in a target system consisting of a silver body and Havar window, as described elsewhere (Kambali et al., 2016). The target was then irradiated with 11 MeV proton beams at a constant integrated beam current of 35 $\mu\text{A}\cdot\text{hr}$. The irradiation procedure was performed using a typical Eclipse 11 cyclotron located at the National Cancer Center (NCC), Dharmais Cancer Hospital in Jakarta, Indonesia, also as previously described (Kambali et al., 2016). During the target bombardment, the pressure inside the cyclotron chamber was kept at 4×10^{-6} mbar, whereas the pressure in the target system was around 30 bar.

2.2. Impurity Analysis

Following the target irradiation, the irradiated target containing F-18 radionuclide was then rinsed and transferred to a lead-shielded container. Subsequently, it was passed through a column in the target transfer system containing Quaternary Methyl Acetate (QMA) resin made by ABX Advanced Biochemical Compounds, Germany. The impurities were measured and analyzed before and after the target passed through the resin. A portable gamma ray spectroscopy system consisting of a pocket MCA (Type MCA8000A) made by Amptek, USA, serial number 2278, coupled to a NaI(Tl) detector, was employed to identify the radioactive impurities present in the target.

2.3. Recoiling and Sputtering Calculations

The behavior of the 11 MeV proton as it passes through the Havar window and in the enriched H_2^{18}O target was simulated using the Stopping and Range of Ions in Matter (SRIM) 2013 codes (Ziegler et al., 2010), whereas the energy of possible atomic impurities recoiled off the Havar window was examined using both the SRIM 2013 calculated data and the atomic collision equation, which has also been applied in deuterium and hydrogen adsorption studies (Kambali

et al., 2008; Gladys et al., 2010; Kambali et al., 2018a; Kambali et al., 2018b; Kambali et al., 2018c). Moreover, collisions between recoiled off cobalt atoms and the silver (Ag) body housing the enriched water target were also simulated to study the origins of the impurities found in the post-irradiated enriched water target. The theoretical calculations were performed using the SRIM 2013 codes, since these have been found to be better at reproducing experimental data than the similar Monte Carlo transport codes, such as FLUKA and MCNPX (Paul, 2006). Other studies have also compared their results with the SRIM-calculated data (Kumar & Diwan, 2015; Pineda-Vargas, 2015; Fontana et al., 2016). Furthermore, the SRIM software was also used to simulate proton range in Nickel target (Suryanto & Kambali, 2018)

3. RESULTS AND DISCUSSION

3.1. Recoiling and Sputtering Calculations

Based on the SRIM-calculated data, the majority of the 11 MeV proton beams (over 99.999%) are transmitted through the 50 μm thick Havar window and consequently hit the enriched water target. The beams lose a total of nearly 3.3 keV as they pass through the Havar foil. The collisions between the 11 MeV protons and the target atoms result in a number of vacancies and displacements, depending on the target atoms. In total, as many as nine atoms in every incoming proton are displaced by the bombardment, meaning nearly 1.97×10^{14} atoms are displaced when an 11 MeV proton beam is directed at the Havar window at a beam current of 35 μA . While the number of displacements is very high, the recoiling atoms may not have enough energy to recoil off or be sputtered off the havar surface. The SRIM-calculated distributions of the recoiling atoms in the Havar foil are shown in Figure 1. The figure indicates that there are significant increases in the recoil yields on the far side of the havar surface (at a distance of 50 μm) which directly touches the enriched water target.

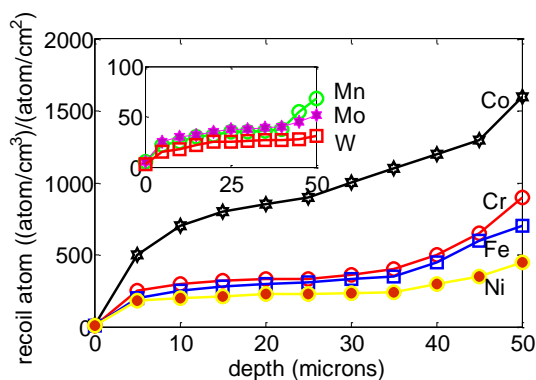


Figure 1 SRIM-calculated recoil distributions of Cr, Fe, Co, Ni, Mn, Mo and W atoms in a 50 μm havar foil

According to the SRIM-calculated data, the individual atoms absorb higher energy from the incoming proton beam than from their surface binding energy, as shown in Table 1, except for C and W atoms. The proton-hit atoms are displaced and then recoil off the Havar window when they absorb enough kinetic energy from the incoming proton beam, as illustrated in Figure 2. The four highest energy absorbers are Co, Cr, Fe and Ni, which indicates that they have the highest chance to be sputtered off the havar surface and to immediately fall into the enriched water target, resulting in detectable atomic species. In some cases, a number of Co, Cr, Fe and Ni atoms could potentially hit the silver (Ag) body, leading to recoiling and sputtering of Ag atoms. The total sputtering yield, expressed in the number of atoms stripped off the havar surface in every incoming proton, is given in Table 1, in which Co atoms represent the highest yield.

Table 1 SRIM-calculated data corresponding to proton-irradiated Havar foil

Atom	Surface binding energy (eV)	Energy absorbed by (eV/ion)	Total sputtering yield (atom/ion)
C	7.41	0	-
Cr	4.12	60	2.24×10^{-7}
Mn	2.98	6	1.71×10^{-8}
Fe	4.34	56	1.79×10^{-7}
Co	4.43	154	4.03×10^{-7}
Ni	4.46	47	1.26×10^{-7}
Mo	6.83	9	1.31×10^{-8}
W	8.68	5	-

While the calculated total sputtering yield of every individual atom is very small, the numbers become significant when the incoming proton beam current is sufficiently high. For instance, when an 11 MeV proton beam is irradiated into the 50 μm thick havar foil at a beam current of 35 μA for 5 minutes, this will correspond to a total of 4.8×10^5 and 2.13×10^5 sputtered Co and Fe atoms respectively. Should the irradiation time be increased to 1 hour, the number of sputtered Co and Fe atoms would be 2.88×10^7 and 1.28×10^7 , respectively, which would be experimentally detectable. However, Co-56 might be the only species observed in the enriched water when the gamma ray spectroscopic system is employed in the measurement. This is due to the fact that $^{56}\text{Fe}(p,n)^{56}\text{Co}$ reaction has the highest nuclear cross section among other havar atoms, as recently discussed by Kambali et al. (2016).

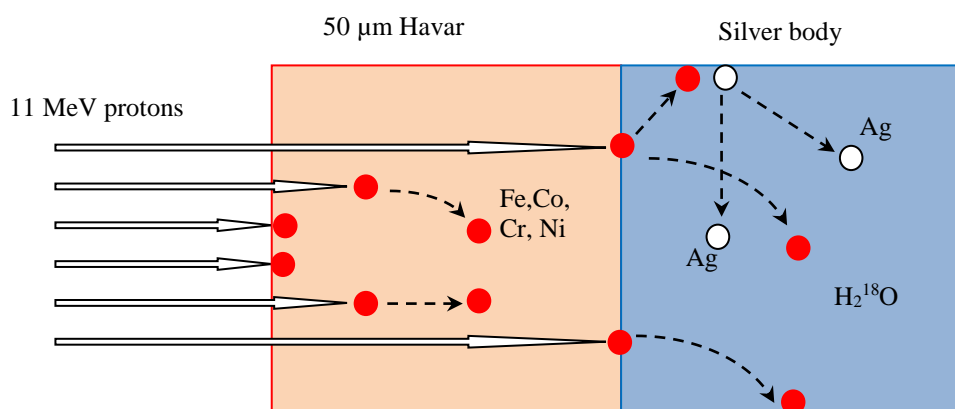


Figure 2 Illustrated trajectories of 11 MeV protons (arrows), displaced and recoiled Havar atoms (●) in a 50 μm Havar window and enriched H_2^{18}O target. This occurrence creates sputtered silver atoms (○)

In the enriched water target, the sputtered Cr, Fe, Co and Ni atoms could lead to further recoiling or sputtering of H and O atoms as they travel through the H_2^{18}O target with the kinetic energy they have obtained from the proton beams. The SRIM-calculated maximum kinetic energy and range of the individual atoms, together with the H and O sputtering yields, are given in Table 2. The table shows that the range of the individual sputtered atoms in the enriched water varies between 6 \AA for Mn and Mo atoms and 40 \AA for Co atoms. In addition, the Co atom collisions with the H_2^{18}O target result in the highest H and O sputtering yields, i.e. 0.0102 H atoms/incident proton and 0.0169 O atoms/incident proton. These values correspond to a total of 1.21×10^{10} recoiled H atoms and 2.01×10^{10} recoiled O atoms when an 11 MeV proton beam is bombarded into the enriched water target at an integrated beam current of 35 $\mu\text{A}\cdot\text{hr}$.

The incoming proton beam also generates H and O recoils, although the yields are insignificant since the (p,n) nuclear reaction between the proton beam and ^{18}O atoms dominates.

Table 2 SRIM-calculated range of Havar-originated atoms in the H_2^{18}O target, together with H and O sputtering yields

Atom	Kinetic energy (eV)	Range in H_2^{18}O (Å)	Sputtering yield (atom/ion)	
			H	O
Cr	55.88	27	0.0005	0.0007
Mn	3.02	6	0	0
Fe	51.66	28	0.0007	0.0004
Co	149.57	40	0.0102	0.0169
Ni	42.54	27	0	0.0001
Mo	2.17	6	0	0
W	0	0	0	0

As mentioned earlier, apart from directly hitting the individual H and O atoms, the recoiling Co, Fe, Ni and Cr atoms could potentially strike the silver body, which eventually leads to the generation of recoiled or sputtered Ag atoms (see Figure 2). The most likely atoms to cause the Ag atoms to recoil off the silver surface are Co atoms, particularly Co-56 ones, since they have the highest kinetic energy and longest range in the enriched water. The SRIM-simulated data at a 45° Co incidence angle shows that 149.57 eV Co atoms could travel as deep as 25 Å through a silver body after passing through a 30 Å thick enriched water target, depending on the incidence angle (Figure 3, inset).

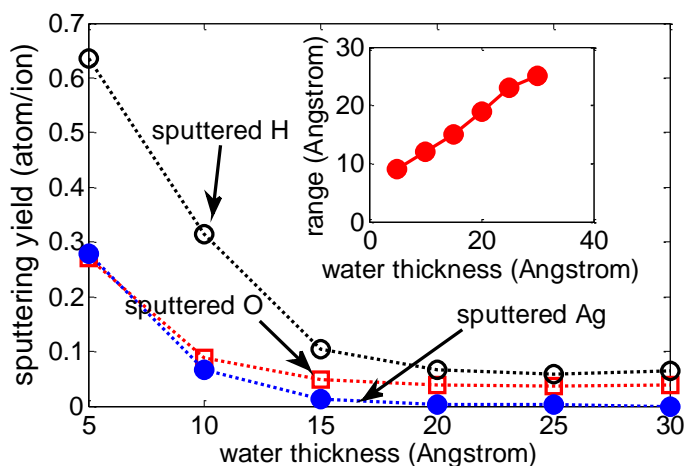


Figure 3 SRIM-calculated sputtering yields of 149.57 eV Co bombarded H, O and Ag atoms at a 45° incidence angle. The range of the 149.57 eV Co atoms in the enriched water target is shown in the inset.

The sputtering yields of H, O and Ag atoms are given in Figure 3, which shows that the yields decrease with increasing water thickness in front of the Co atoms. As many as 0.28 Ag atom is sputtered off the silver surface in every incoming Co atom when the Co atom hits the silver body after passing through 5 Å thick water. The yield falls to 0.002 atom/ion as the Co atoms travel through 30 Å thick water. Such yields will result in experimentally detectable sputtered Ag atoms in the enriched water target. Note that the sputtered Ag atoms may also come from the Co-hit Ag surface at other incidence angles, which suggests a higher probability of experimentally observed Ag atoms in the enriched water target.

3.2. Experimental Spectrum of F-18 and Radionuclidic Impurities

Based on the experimental data, irradiation of the H_2^{18}O target using 11 MeV proton beams at an integrated beam current of 35 μA for 5 minutes results in total radioactivity of nearly 100 mCi, or around 34.65 mCi/ $\mu\text{A}\cdot\text{hr}$. The F-18 spectrum captured from the irradiated H_2^{18}O target is given in Figure 4, which shows an extremely strong gamma ray peak at 0.511 MeV. The unstable F-18 radionuclide emits a positron (β^+), which immediately interacts with free electron, resulting in annihilation of the two particles and eventually giving rise to the pronounced peak at 0.511 MeV. The emitted gamma ray hits surrounding materials such as the lead shield and then scatters back into, and is recognized by, the NaI(Tl) detector as a backscattered peak at around 0.17 MeV.

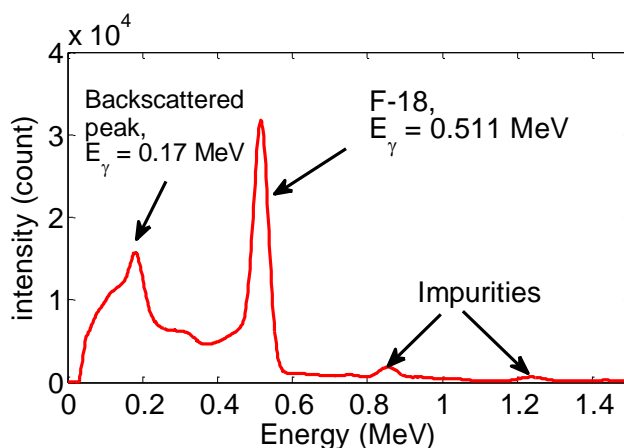


Figure 4 Spectrum of the F-18 radionuclide observed shortly after the end of proton irradiation of the enriched water target

Apart from the annihilation peak, there are also a few peaks which are nearly invisible at gamma energy of between 0.6 and 1.5 MeV. For better analysis of the radioactive recoils present in the irradiated water, the sample was cooled for a day to allow the F-18 radionuclide to decay. As can be seen from Figure 5, two photoelectric peaks are observed at $E_\gamma = 0.847$ and 1.238 MeV, which both correspond to Co-56 gamma ray emissions (half-life = 77.3 days). In addition, there are also three weak photoelectric peaks at $E_\gamma = 0.658$, 0.885 and 1.4 MeV, which are emitted by the Ag-110m radioisotope (half-life = 249.8 days).

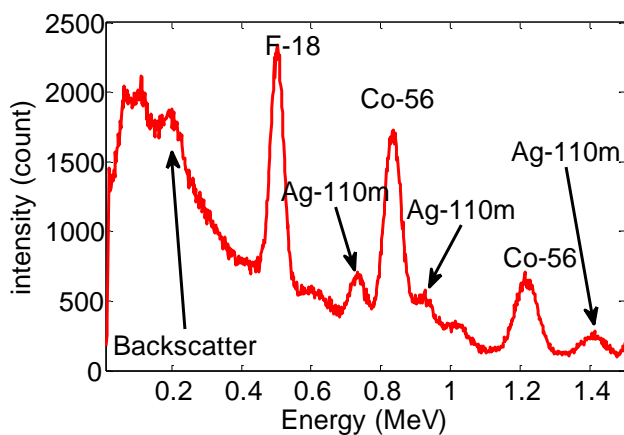


Figure 5 Gamma ray spectrum of impurities present in the irradiated H_2^{18}O target, observed following a day of decay

The Co-56 impurity is presumably from the Havar window, produced via $^{56}\text{Fe}(p,n)^{56}\text{Co}$ nuclear reaction and falling into the irradiated water, as predicted by the SRIM-calculated results. This corresponds well with an earlier Havar foil observation made by Kambali et al. (2016). The presence of Co-56 in the post-irradiated water target indicates that during the proton bombardment, the Co-56 radionuclidic impurity recoils off the havar surface and then promptly falls into the water, as discussed in Section 3.1. Other radionuclidic impurities, such as V-48, Cr-51, Mn-52, Mn-54, Co-57 and Co-58, detected earlier by Köhler et al. (2013), are not found in this study, mainly due to the lower proton energy (11 MeV) employed in this investigation compared to previous studies, which used up to 18 MeV protons (Bowden et al., 2009).

The silver body housing the enriched water target was also being activated by the secondary neutrons generated from the proton irradiation via $^{109}\text{Ag}(n,\gamma)^{110\text{m}}\text{Ag}$ nuclear reaction, as discussed elsewhere (Kambali et al., 2016; Bowden et al., 2009). The detected Ag-110m radioactivity in the irradiated water target is also evidence that the silver atoms are sputtered off the surface, most likely by Co atoms originating from the havar window, as discussed in Section 3.1.

Before using the ^{18}F solution to label the FDG samples, the radioactive solution was assessed for its radionuclidic impurity contents after introducing it into a QMA column. The gamma ray spectrum of the ^{18}F solution shortly after passing through the QMA column, the QMA column itself, and the ^{18}F solution after a 3-day cooling period are shown in Figure 6. The figure indicates that the gamma ray intensity of the F-18 radionuclide remains strong, although the positron-emitting radionuclide is also adsorbed by the QMA column as it is transferred through the column. Moreover, no significant amounts of radionuclidic impurities are found in the ^{18}F solution. Radionuclidic impurities such as Co-56 and Ag-110m are adsorbed by the QMA column, as shown by their gamma ray spectrum recorded in the column (Figure 6, inset), in which around 15% Co-56 and 64% Ag-110m of their original EOB yields are observed in the column, respectively. There remain some significant amounts of Co-56 and Ag-110m impurities observed in the ^{18}F solution following the 3-day cooling or decay period.

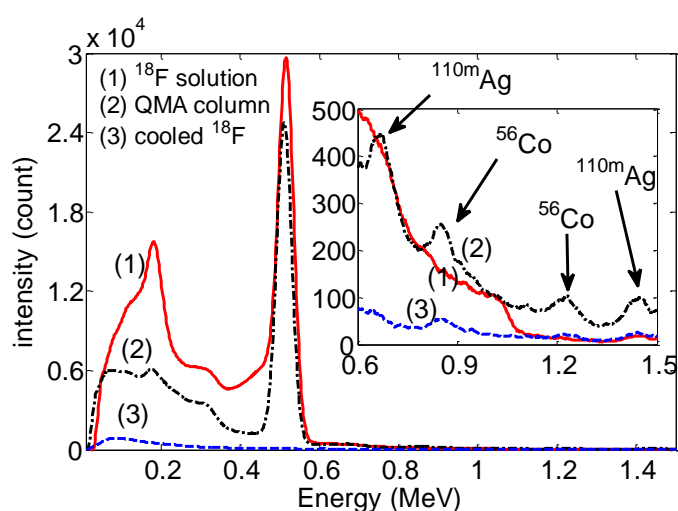


Figure 6 Gamma ray spectrum captured in the (1) ^{18}F solution, (2) QMA column and (3) ^{18}F solution following 3 days of decay

The existence of impurities is always an issue in radionuclide production. Future studies on adsorption of such impurities could be conducted using banana peel and coconut shell, as previously investigated for the adsorption of Ni ions (Olufemi et al., 2018), as well as analysis of solutions in multicomponent systems using activated carbon from banana peels for the

adsorption of lanthanide ions (Kusrini et al., 2018), so that the impurity issue in F-18 radionuclide production can be solved.

4. CONCLUSION

A theoretical and experimental study of recoiled and sputtered radionuclidic impurities has been conducted. The SRIM codes have been employed to study the recoil distributions, kinetic energy and sputtering yields of individual Havar atoms, a silver body and an enriched H₂¹⁸O target. Based on the SRIM-calculated results, the Co, Cr, Fe and Ni recoil yields increase near the far side of the Havar surface (at a distance of 50 μm), which directly touches the enriched water target. These atoms have the highest probabilities of being recoiled off the Havar surface and then falling into the enriched water target or even hitting the silver body, which could result in further sputtering of the Ag atoms. The experimental data indicate that Havar window-originated ⁵⁶Co atoms and silver body-originated ^{110m}Ag atoms are identified in the post-irradiated water target, although a significant presence in the ¹⁸F solution is no longer observed after passing it through a QMA column. The impurities remain detectable in the ¹⁸F solution after a 3-day cooling period. Future work will concentrate on the measurement of non-radioactive recoiled and sputtered atoms in the enriched water target, as well as adsorption of the impurities.

5. ACKNOWLEDGEMENT

This research project is supported by The World Academy of Sciences (TWAS) under the Principal Investigator's Research Grant Number 15-020 RG/PHYS/AS_I – FR3240287075, as well as the Indonesian National Nuclear Energy Agency (BATAN). Moreover, kind support from the Dharmais Cancer Hospital has also greatly contributed to the success of the project. Technical support from the cyclotron technicians and staff at Dharmais Cancer Hospital in Jakarta is also gratefully acknowledged.

6. REFERENCES

- Bowden, L., León Vitró, L., Mitchell, P.I., O'Donnell, R.G., Seymour, A.M., Duffy, G.J., 2009. Radionuclide Impurities in Proton-irradiated [¹⁸O]H₂O for the Production of ¹⁸F-: Activities and Distribution in the [¹⁸F]FDG Synthesis Process. *Applied Radiation and Isotopes*, Volume 67(2), pp. 248–255
- Fontana, C.L., Chen, C., Crespillo, M.L., Graham, J.T., Xue, H., Zhang, Y., Weber, W.J., 2016. Stopping Power Measurements with the Time-of-Flight (ToF) Technique. *Nuclear Inst. and Methods in Physics Research B*, Volume 366, pp. 104–116
- Gladys, M.J., Kambali, I., Karolewski, M.A., Soon, A., Stampfl, C., O'Connor, D.J., 2010. Comparison of Hydrogen and Deuterium Adsorption on Pd(100). *The Journal of Chemical Physics*, Volume 132(2), pp. 024714-1–024714-8
- Hjelstuen, O.K., Svadberg, A., Olberg, D.E., Rosser, M., 2011. Standardization of Fluorine-18 Manufacturing Processes: New Scientific Challenges for PET. *European Journal of Pharmaceutics and Biopharmaceutics*, Volume 78(3), pp. 307–313
- Je, H., Ahn, L.B., Lee, J., 2012. The Usefulness of F-18 Fluorodeoxyglucose Positron Emission Tomography/computed Tomography in Patients with Langerhans Cell Histiocytosis. *Annals of Nuclear Medicine*, Volume 26(9), pp. 730–737
- Jung, K., Lee, J.H., Park, J.W., Moon, S., Cho, Y.S., Choe, Y.S., Lee, K., 2016. Effects of Curcumin on Cancer Cell Mitochondrial Function and Potential Monitoring with ¹⁸F-FDG Uptake. *Oncology Reports*, Volume 35(2), pp. 861–868
- Kambali, I., 2018a. Production of Lu-177 Radionuclide using Deuteron Beams: Comparison between (d, n) and (d, p) Nuclear Reactions. *Journal of Physics: Conference Series*, Volume 1120, pp. 012010

- Kambali, I., 2018b. Cyclotron-based Samarium-153 Production using Alpha Particle Beam Irradiation. *Journal of Physics: Conference Series*, Volume 1120, pp. 012010
- Kambali, I., 2018c. Calculated Astatine-211 Production Yields for Radioimmunotherapy. *Journal of Physics: Conference Series*, Volume 1116, pp. 032013
- Kambali, I., Connor, D.J.O., Gladys, M.J., Karolewski, M.A., 2008. Determination of Deuterium Adsorption Site on Palladium(100) using Low Energy Ion Recoil Spectroscopy. *Applied Surface Science*, Volume 254(14), pp. 4245–4250
- Kambali, I., Heryanto, T., Rajiman, Ichwan, S., 2011 Reliability Study of the Liquid Target Chamber for F-18 Production at the BATAN's Cyclotron Facilities. *Atom Indonesia*, Volume 37(1), pp. 5–10
- Kambali, I., Suryanto, H., Parwanto, 2016. Radioactive by-products of a Self-shielded Cyclotron and the Liquid Target System for F-18 Routine Production. *Australasian Physical and Engineering Sciences in Medicine*, Volume 39(2), pp. 403–412
- Köhler, M., Degering, D., Zessin, J., Füchtner, F., Konheiser, J., 2013. Radionuclide Impurities in [18F]F and [18F]FDG for Positron Emission Tomography. *Applied Radiation and Isotopes*, Volume 81, pp. 268–271
- Kumar, S., Diwan, P.K., 2015. Energy Loss and Straggling of a Particles in Ag and Sn Metallic Foils. *Journal of Radiation Research and Applied Sciences*, Volume 8, pp. 538–543
- Kusrini, E., Kinastiti, D.D., Wilson, L., Usman, Rahman, A., 2018. Adsorption of Lanthanide Ions from Aqueous Solution in Multicomponent Systems using Activated Carbon from Banana Peels (*Musa paradisiaca* L.). *International Journal of Technology*, Volume 9(6), pp. 1132–1139
- Lemaire, C., Libert, L., Franci, X., Genon, J., Kuci, S., Giacomelli, F., 2015. Automated Production at the Curie Level of No-carrier-added 6-[18F] Fluoro-L-dopa and 2-[18F] Fluoro-L-tyrosine on a FASTlab Synthesizer. *Journal of Labelled Compounds and Radiopharmaceuticals*, Volume 58(7), pp. 280–291
- Libert, L.C., Franci, X., Plenevaux, A.R., Ooi, T., Maruoka, K., Luxen, A.J., Christian, F., 2014. Production at the Curie Level of No-carrier-added 6-18F-Fluoro-l-dopa. *Journal of Nuclear Medicine*, Volume 54(7), pp. 1154–1161
- Olufemi, B., Eniodunmo, O. 2018. Adsorption of Nickel(II) Ions from Aqueous Solution using Banana Peel and Coconut Shell. *International Journal of Technology*, Volume 9(3), pp. 434–445
- Paul, H., 2006. A Comparison of Recent Stopping Power Tables for Light and Medium-heavy Ions with Experimental Data, and Applications to Radiotherapy Dosimetry. *Nuclear Inst. and Methods in Physics Research B*, Volume 247(2), pp. 166–172
- Pineda-Vargas, C., 2015. Energy Loss Measurements of ⁶³Cu, ²⁸Si and ²⁷Al Heavy Ions Crossing Thin Polyvinylchloride (PVC) Foil. *Nuclear Inst. and Methods in Physics Research B*, Volume 363, pp. 24–27
- Suryanto, H., Kambali, I., 2018. A Novel Method for Ni-57 and Co-57 Production using Cyclotron-generated Secondary Neutrons. *Atom Indonesia*, Volume 44, pp. 81–87
- Xie, C.H., Hsu, W.L., Xie, H.L., Lin, M.C., Lan, W.C., Chao, H.Y., 2011. GMP Production of [18F] FDOPA and Issues Concerning Its Quality Analyses as in USP "Fluorodopa F-18 Injection". *Annals of Nuclear Medicine*, Volume 25(5), pp. 309–316
- Ziegler, J.F., Ziegler, M.D., Biersack, J.P., 2010. The Stopping and Range of Ions in Matter (2010). *Nuclear Inst. and Methods in Physics Research B*, Volume 268, pp. 1818–1823